Fluidisation due to wave loading (one dimensional solution)

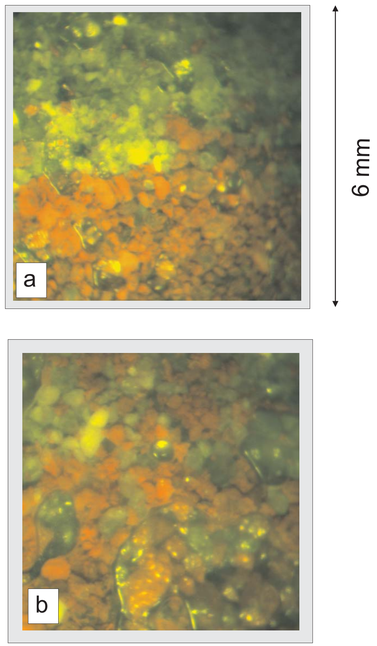

Figure 2. Images taken by endoscopic investigations of a non-fluidised (a) and fluidised (b) soil region

Irreversible mixing of color coated sediment layers have been observed using an endoscopic image processing techique. Starting from an initially distinct separation (Fig 2a), the two sand layers (mean diameter of 0.2 mm) increasingly mixed with the number of load cycles (Fig 2b).

Possible soil bed deformations in an unsaturated submerged soil may be caused by external pressure changes such as unloading due to rapid water level draw down. The impact of such loading will become even more dangerous with cycling pressures or oscillating water levels. Heaving, settling and fluidisation of the sand bed may happen, causing solid grain structure deformation and soil failure. Figure 2 shows the results of the computed pore pressure response and the induced transient seepage velocities at different depth levels in a 2 m thick soil bed, induced by a sinusoidal wave loading acting on a shallow sea bed of about 4 m water depth. The material of the soil bed consists of uniform sand with a permeability of $k = 2.5 \times 10^{-5}$ m/s. The wave used had a period of 5 s, a wave height of 2.4 m and a propagating velocity of 5 m/s. Due to the frequency of the acting pressure oscillation the pore pressure response is delayed by a phase shift of the pressure amplitudes of some 0.5 s and a pressure damping with increasing soil depth (Figure 3a). The onset of fluidisation at a depth of 0.28 m below sea bed becomes evident by the repeated occurrence of constant flow velocity at transient state, every time during the unloading stage of the wave. It is worth noticing, that in stages in which fluidisation (liquefaction) occurs, opposite flow direction exists simultaneously in different soil depth levels. In the upper soil layer the flow is governed by the actual loading and in the lower ones the water is still flowing in the opposite direction (see arrows in Figure 3b).

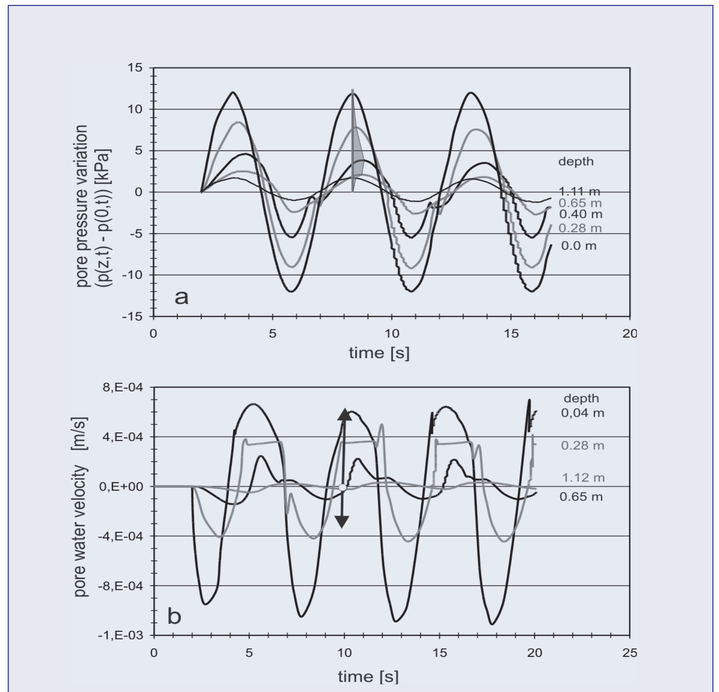

Figure 3. History of pore pressure and pore water velocity for wave loading (1D simulation)

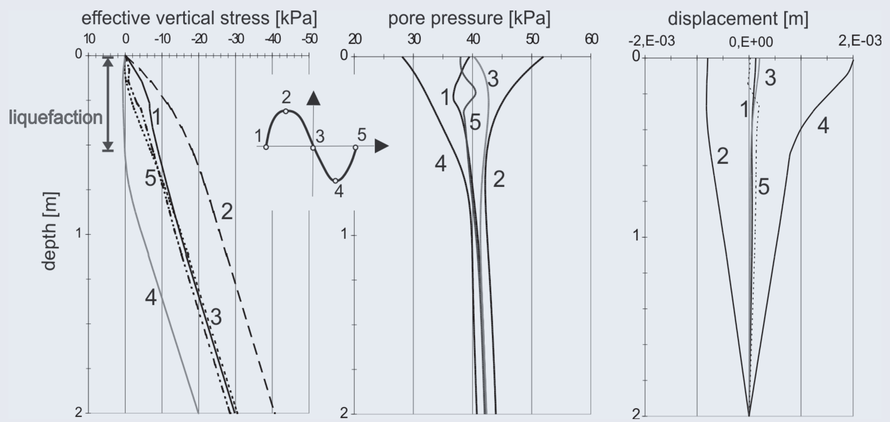

Figure 4. Distribution of vertical effective stresses (a), pore pressure (b) and displacements (c) under wave loading (1D simulation)

Vertical distributions of the effective vertical stress, pore pressure and displacement are presented in Figure 4 at different loading stages. The depth of the liquefied strata is restricted to the upper soil layers (up to no more than 0,5 m - at loading stage 2). The pore pressure distribution is still disturbed by fluidisation even in the neutral loading stages 1, 3 and 5. As expected, larger displacements occur in the liquefied soil areas. The depth of the fluidised (liquefied) soil area is marked by the arrow describing the liquefaction depth of about 0.5 m below sea bed.

Fluidisation due to travelling waves (two dimensional solution)

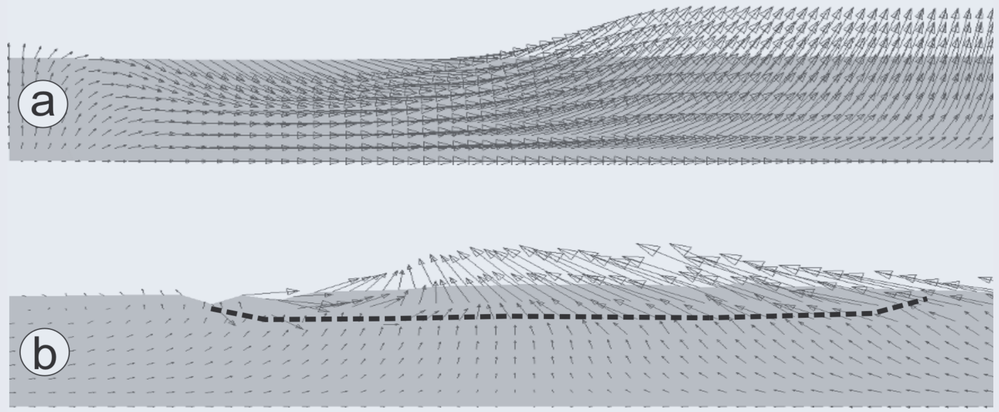

Figure 5. Displacement fields at elastic (a) and liquefied (b) stages (2 D simulation, different vector scale used)

The one-dimensional investigation neglects the influence of horizontal soil displacements caused by propagating waves. In order to prove these effects two-dimensional analyses were performed. The former described wave characteristics have been used.
The compressibility of near saturated soils is governed by the time dependant stress distribution between the solid phase and the compressible water-air mixture. The compressibility of the fluid was expressed in the degree of saturation S, the water compressibility , the volumetric coefficient of air solubility h and the environmental pressure p (Bishop & Eldin 1950):

$$S_w \quad \frac{1 \quad S \quad hS}{p}$$

As expected, in the case when the liquefaction takes place (Figure 5b), the soil particle trajectories are no longer elliptically shaped. The movement amplitude is up to four times larger and directed against the propagating wave.
The soil model has two possible states: solid or fluidised (liquefied). The liquefaction takes place, where the vertical water pressure gradient exceeds the unit weight of the soil. Actually the liquefaction is a stress-softening process and instabilities are related with the FE simulation (Bardet 1996). In order to have some extent of control on the numerical instabilities an explicit procedure with a corresponding time stepping control has been implemented.
Figure 5 describes the displacement fields for two models: in the first model (a) a linear elastic soil behaviour was adopted. In the second model (b) the soil is allowed to behave viscous and fluidisation may occur.

An interesting result of the simulations is presented in Figure 6. In the upper figure part (a) a snapshot of the pore water velocity field is shown and in the lower part (b) the associated flow direction is described. The loading part of the travelling wave acts at the right hand side of Figure 6, whilst the left edge shows liquefaction due to action of the unloading part of the wave. In the loading domain the water flow is converging due to the superposition of two simultaneously acting flows. The still upward directed flow in the depth caused by the precedent unloading wave part is already covered up by the simultaneously initiated downward flow caused by the loading wave part.

In the liquefied zone a divergent water flow can be observed. The water in the upper part is already moving up-wards whilst in the lower part the flow remains downward directed. The borderline indicates the limit of the liquefied zone.

Each time effective stress is substantially reduced by wave loading causing transient excess pore pressures, soil particle transport may easily be induced. Due to the loss of the inter-granular friction during the liquefaction of the soil an enhanced erosion of the soil bed can be observed, when a horizontal current is present. Transient sand bed deformations, such as the development of sand waves, will take place at the sea bed. The formed sand beds will of course disintegrate by a following change in water loading characteristics (decreasing amplitudes, propagating velocities and wave length).

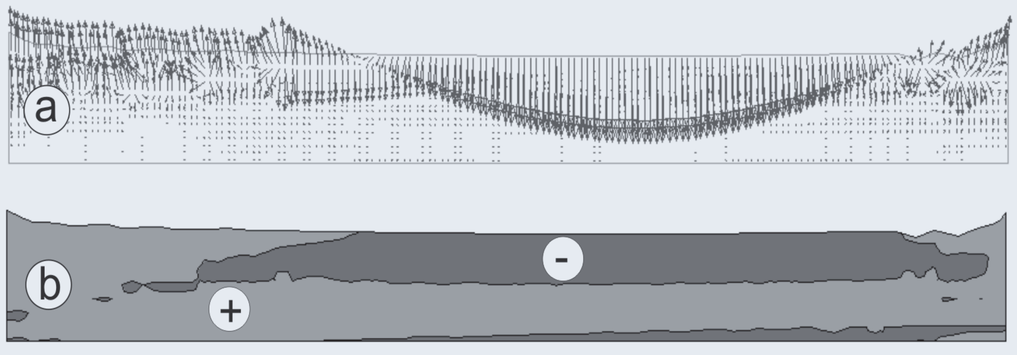

Figure 6. Pore water velocity field (a) and areas with upward (+) and downward (-) flow caused by traveling vawes (2D)

Hydraulic failure and soil-structure deformation due to wave and draw down loading

Coastal Structures 2003 Conference, 26th - 29th August 2003, Portland, Oregon (USA)

Köhler, H.-J. & Schwab, R.
Federal Waterways Engineering and Research Institute, Karlsruhe, Germany
Geotechnical Department
e-mail: koehler@baw.de or schwab@baw.de
Davis, M. & Koenders, M. A.
Kingston University, Kingston on Thames, UK
Department of Mathematics,
e-mail: mast@kingston.ac.uk or koenders@kingston.ac.uk

ABSTRACT: In engineering practice soils under water are commonly considered to be saturated and the pore fluid is rated being incompressible. In shallow water depth this two-phase model is no longer consistent with natural conditions. Even smallest quantities of gas bubbles change the properties of the pore fluid dramatically. Due to external fluctuating pressures, the gas bubbles inside the gas-water mixture attempt to counteract such external pressure variations by volume changes, thus causing local transient micro flow. This process is hampered by low permeability. On the basis of Biot's consolidation equation, using coupled and uncoupled numerical simulations, it can be demonstrated, that oscillating pressure loading contributes to soil deformation, fluidisation and hydraulic failure at transient pore pressure state. Due to the natural gas content of the pore fluid, external pressure changes may induce volume changes of the entrapped gas bubbles causing soil deformation and even soil failure. Different failure mechanisms may be observed. Investigating loading factors such as rapid draw down or wave loading and turbulent water current acting on a protected or unprotected sandy soil bed at shallow water conditions, the actual pore pressure response of the submerged subsoil may be calculated. It is demonstrated, that this loading contributes to sand bed deformation, fluidisation and hydraulic failure. Enhanced erosion and scouring may take place.

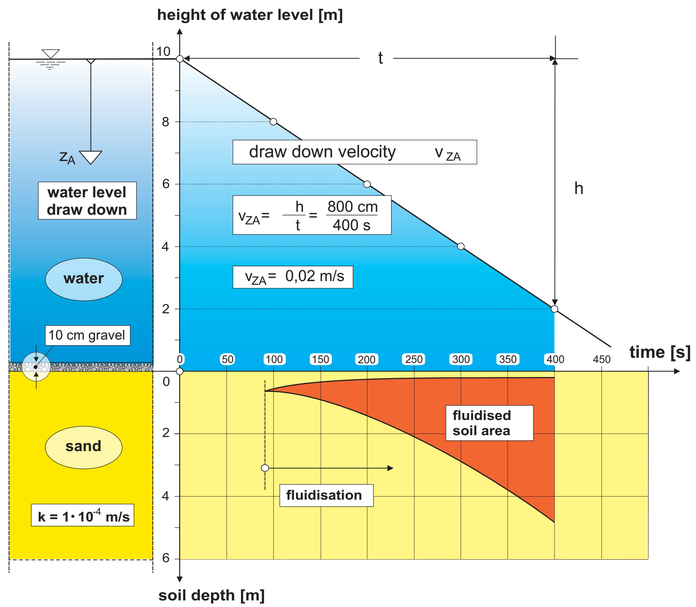

Figure 1: Fluidised soil area due to draw down

Fluidisation due to draw down loading

Example:
A partially saturated sandy sea bed at 10 m water depth is protected by a 10 cm thick gravel layer, acting as a top load in order to prevent current induced soil erosion. Water level draw down loading at a constantly falling rate of v_{zA} = h/ t [m/s], greater than the permeability k [m/s] of the submerged subsoil, may easily induce fluidisation as soon as a certain draw down level has been reached. At a critical depth below the protection layer the soil starts to fluidise. With an ongoing continuous falling of the external water pressure exceeding the critical time, when fluidisation started at first to occur at critical depth, the endangered soil area continues to increase, reaching down to a depth of about 5 m, whilst the water level draw down level has already increased to h = 8 m below the initial water head of 10 m (see Figure 1).

Two fluidising front lines may develop. One is reaching far down into the subsoil, the other one is developing above the initially induced fluidisation zone at critical time and critical soil depth increasing in height, but not touching the interface between the overtopping gravel layer and the sandy subsoil. In between both fluidising front lines the overall incorporated soil area of the fluidised soil region is plotted as a function of time (see Figure 1). The soil in the fluidised area shows a high viscous behaviour. In the shown example the velocity v_{zA} = 0.02 m/s of the external water level lowering exceeds the governing water permeability of the sand (k = 1 x 10^{-4} m/s) by about two orders of magnitudes. In case the velocity of the water level lowering v_{zA} would be smaller than the governing permeability of the subsoil, the sand would not fluidise. Where no top load is present, fluidisation takes place earlier and starts directly at the interface water/sand. If one expects an external pressure fall at the rate of v_{zA} to continue for a time less than critical time step, then the bed will also not fluidise (*Köhler & Koenders, JHR 2003, Volume 41, No. 1, p. 69 -78 and Roussel et al., Proc. of Geofilters 2000, Balkema, p.75 - 82*)

Turbulent current acting on a protected or unprotected river bed (Lattice Boltzman Simulation)

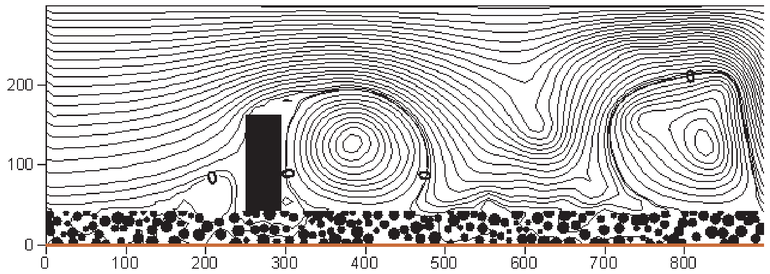

Figure 7. Snapshot of the flow lines as a function of the position for the case of flow over an obstacle

As for variations in the conditions in the open water and coarse layer, new simulations would have to be carried out to study the effects of independent parameter changes such as particle size and distribution of the coarse layer, dimensions and shape of the obstacle (including attempts to streamline it) as well as different mean flow velocities. An extension of the method to three dimensions is possible, but is not realistically taken into consideration because of the substantially greater computer power required. This problem is in common with all high Reynolds number simulations. The dimensions that are being used in the above calculations are suitable for predicting the pore pressure characteristics in model tests. It is quite straightforward to obtain predictive results for prototype conditions, as the usual fluid mechanics dynamic similarity rules apply.

In order to ascertain erosion sensitivity the direction of the excess pore pressure gradient is important. The illustration in Figure 8 shows that the region that is most prone to a rate of change of pore pressure variation is behind the obstacle. Here the pore pressure gradient oscillates with the passing of the rolling eddies. The results obviously depend on the choice of the parameters of the problem. For conditions that are relevant to model testing with a rectangular obstacle it is shown that the excess pore pressure variations in the subsoil vary with time, making a region behind the obstacle vulnerable to erosion damage (Davis et al., 2003).

Flow is considered over an obstacle placed on a coarse gravel layer that covers a sand layer (Figure 7). The pressure distribution as a function of position and time is obtained for partially saturated conditions in the subsoil (Figure 8). The flow in the open water and coarse layer is calculated using a lattice Boltzmann technique; the pressure in the subsoil is evaluated by means of an analytical solution using the lattice Boltzmann simulation as boundary condition. The results demonstrate where the greatest risk of damage to the subsoil may be located. It is emphasised that this is an illustration of the technique, employing lattice Boltzmann simulation in the open water and in the coarse layer and calculating the excess pore pressures in the subsoil by means of an analytical model, appropriate to partially saturated conditions. Various extensions include parameter sensitivity studies. Insofar as the subsoil is concerned, these may be carried out with relative ease, because the same lattice Boltzmann simulation boundary condition results can be used to study the pore pressure response, following the the ideas presented by Köhler & Koenders (2003, JHR, Vol. 41, 1).

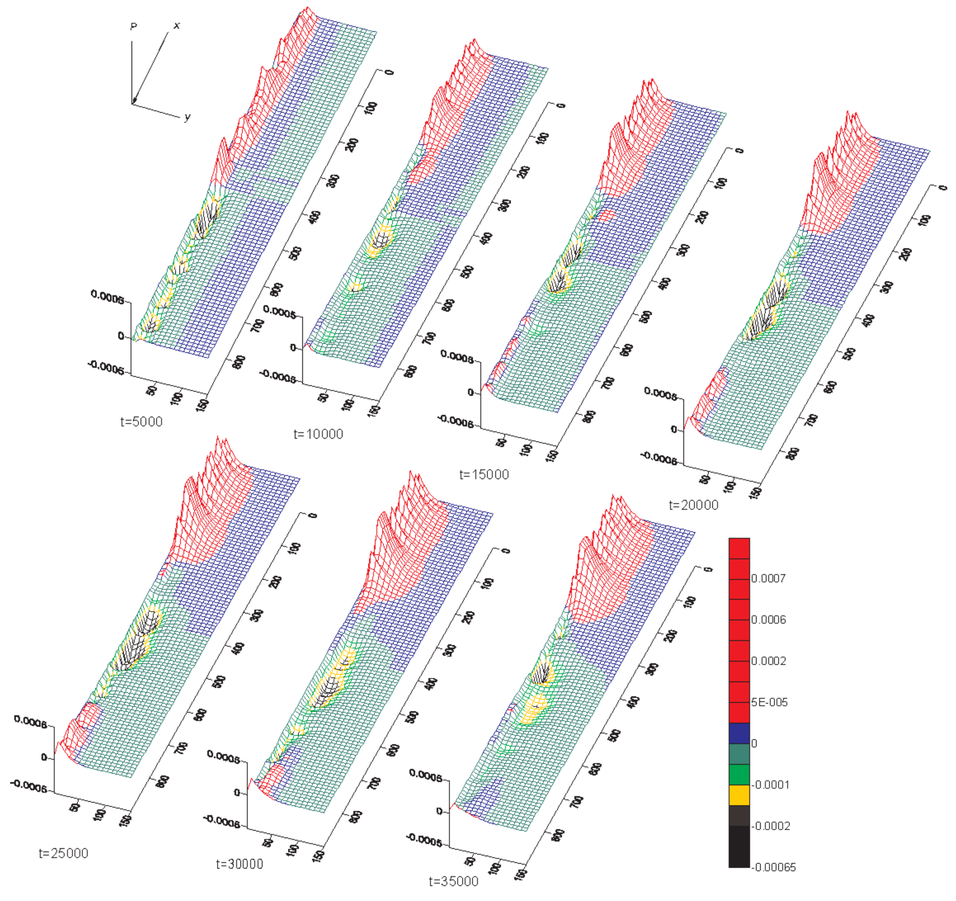

Figure 8. Illustration of a sequence of excess pore pressure profiles at different time stages. Direction of flow is the x-axis, y-axis is depth of sand and P is pressure inside the sand.